

Supplementary Materials for “Higher-order Skin Effect and Its Observation in an Acoustic Kagome Lattice”

Jia-Xin Zhong^{*1}, Pedro Fittipaldi de Castro^{*2}, Tianhong Lu², Jeewoo Kim¹, Mourad Oudich^{1,3}, Jun Ji¹, Li Shi⁴, Kai Chen⁴, Jing Lu^{†4}, Yun Jing^{‡1}, and Wladimir A. Benalcazar^{§2}

¹Graduate Program in Acoustics, The Pennsylvania State University, University Park, PA 16802, USA

²Department of Physics, Emory University, Atlanta, Georgia 30322, USA

³Université de Lorraine, CNRS, Institut Jean Lamour, F-54000 Nancy, France

⁴Key Laboratory of Modern Acoustics and Institute of Acoustics, Nanjing University, Nanjing 210093, China

January 7, 2025

Contents

Supplementary Notes	2
S1 Correspondence between zero states of chiral-symmetric Hermitian systems and skin effect of non-Hermitian systems	2
S2 Topological invariants of C_n- and time-reversal-symmetric non-Hermitian lattices	3
S3 The coupled-model theory for the unidirectional coupling of two coupled acoustic cavities	6
Supplementary Figures	7
Supplementary Movies	11
References	13

^{*}These two authors contributed equally.

[†]lujing@nju.edu.cn

[‡]yqj5201@psu.edu

[§]benalcazar@emory.edu

Supplementary Notes

S1 Correspondence between zero states of chiral-symmetric Hermitian systems and skin effect of non-Hermitian systems

We show with a specific example in one dimension how the presence of topologically protected zero states in a Hermitian chiral-symmetric Hamiltonian H is connected to the existence of a skin effect on its non-Hermitian counterpart Q . Consider the SSH model,

$$H = \sum_n \kappa b_n^\dagger a_n + a_{n+1}^\dagger b_n + \text{h.c.}, \quad (\text{S1})$$

where $a(a_n^\dagger)$ and $b(b_n^\dagger)$ are the particle annihilation (creation) operators of sublattices A and B , respectively, at unit cell $n = 1, 2, \dots, L$. The parameter $\kappa > 0$ controls the intra-cell hopping, while the inter-cell hopping strength is set to 1. The Hamiltonian (S1) is Hermitian and chiral-symmetric. When $\kappa < 1$, the system is in a topologically nontrivial phase characterized by a winding number $w = 1$ under periodic boundary conditions (PBC) and by two exponentially localized states under open boundary conditions (OBC) at the left and right boundaries which have zero energy in the limit $L \rightarrow \infty$, whereas for $\kappa > 1$, the winding number vanishes and there are no chiral zero states. Let us express the degrees of freedom using the vector notation $(\mathbf{a}; \mathbf{b}) \equiv (a_1, a_2, \dots, a_L; b_1, b_2, \dots, b_L)$, where the first (last) L components are operators acting on sublattice A (B). In this basis, the Hamiltonian (S1) takes the form of an off-diagonal $2N \times 2N$ matrix:

$$H = (\mathbf{a}^\dagger \quad \mathbf{b}^\dagger) \begin{pmatrix} 0 & Q \\ Q^\dagger & 0 \end{pmatrix} \begin{pmatrix} \mathbf{a} \\ \mathbf{b} \end{pmatrix}. \quad (\text{S2})$$

From (S2), one may check that the zero mode located at the left (right) edge has support exclusively over the A (B) sublattice

$$|L\rangle = \sum_n \phi_n a_n^\dagger |0\rangle, \quad |R\rangle = \sum_n \psi_n b_n^\dagger |0\rangle, \quad (\text{S3})$$

where $|0\rangle$ is the system's ground state and

$$Q = \begin{pmatrix} \kappa & 0 & 0 & \cdots \\ 1 & \kappa & 0 & \\ 0 & 1 & \kappa & \\ \vdots & & & \ddots \end{pmatrix} \quad (\text{S4})$$

is a non-Hermitian $L \times L$ matrix that couples sublattices A and B . Mathematically, such a matrix is identical to the Hamiltonian of a different physical system defined on a lattice with L sites, that is, half the size of the original SSH system. One can establish a physical interpretation of the new system by defining the operators acting on a new lattice as $c_n^\dagger \equiv a_n^\dagger$ and $c_n \equiv b_n$, such that (S4) under OBC effectively becomes

$$Q = \kappa \sum_{n=1}^L c_n^\dagger c_n + \sum_{n=1}^{L-1} c_{n+1}^\dagger c_n. \quad (\text{S5})$$

The expression (S5) is similar to the Hamiltonian of the Hatano-Nelson (HN) model [1, 2], and describes a one-dimensional lattice with an on-site energy term κ and a unidirectional hopping to the right with strength equal to 1. Following reference [3], let us show that such a system hosts the skin effect. Consider a slightly modified

version of (S5),

$$Q_\epsilon = \kappa \sum_{n=1}^L c_n^\dagger c_n + \sum_{n=1}^{L-1} \left(c_{n+1}^\dagger c_n + \epsilon c_n^\dagger c_{n+1} \right), \quad (\text{S6})$$

where $0 < \epsilon < 1$ (we may take the limit $\epsilon \rightarrow 0$ in the end of the calculation). Now, let us implement the following similarity transformation (imaginary gauge transformation), which is applicable under OBC:

$$V_r^{-1} c_n V_r = r^{-n} c_n, \quad V_r^{-1} c_n^\dagger V_r = r^n c_n, \quad (\text{S7})$$

so that (S6) transforms as

$$V_r^{-1} Q_\epsilon V_r = \kappa \sum_{n=1}^L c_n^\dagger c_n + \sum_{n=1}^{L-1} \left(r c_{n+1}^\dagger c_n + \epsilon r^{-1} c_n^\dagger c_{n+1} \right). \quad (\text{S8})$$

If we choose $r = \sqrt{\epsilon}$, the transformed Hamiltonian becomes Hermitian:

$$V_{\sqrt{\epsilon}}^{-1} Q_\epsilon V_{\sqrt{\epsilon}} = \kappa \sum_{n=1}^L c_n^\dagger c_n + \sqrt{\epsilon} \sum_{n=1}^{L-1} \left(c_{n+1}^\dagger c_n + c_n^\dagger c_{n+1} \right). \quad (\text{S9})$$

Due to its Hermiticity, the spectrum is real and the identical under OBC or PBC:

$$E(k) = \kappa + 2\sqrt{\epsilon} \cos k, \quad k \in [-\pi, \pi]. \quad (\text{S10})$$

Crucially, a similarity transformation does not change the eigenvalues of a matrix, so (S10) is also the spectrum of the non-Hermitian Hamiltonian (S6) under OBC. Moreover, since the transformed Hermitian Hamiltonian (S9) has delocalized eigenstates, all the eigenstates of (S6) are localized at the right edge as $\sim e^{(n-L)/\xi}$ with $\xi = (\log \sqrt{\epsilon})^{-1}$, which constitutes the skin effect [3]. By taking the unidirectional hooping limit $\epsilon \rightarrow 0$, we find that the eigenstates of (S5) are maximally localized at site $n = L$. Conversely, the eigenstates of its Hermitian conjugate Q^\dagger are localized at the left edge of the system.

S2 Topological invariants of C_n - and time-reversal-symmetric non-Hermitian lattices

In this section, we construct the topological invariants that classify the high-order topological phases of non-Hermitian Hamiltonians with spinless time-reversal symmetry (TRS),

$$\Theta h(\mathbf{k}) \Theta^{-1}, \quad (\text{S11})$$

where Θ represents complex conjugation and obeys $\Theta^2 = 1$, and with a crystalline C_n symmetry:

$$r_n h(\mathbf{k}) r_n^\dagger = h(R_n \mathbf{k}), \quad (\text{S12})$$

where r_n is the $2n$ -fold rotation operator satisfying $(r_n)^n = I_{N \times N}$ and R_n is the n -fold rotation matrix acting on the momentum vector \mathbf{k} .

We know that the rotation operator commutes with the Hamiltonian at the high-symmetry points (HSPs) $\Pi^{(n)}$ of the Brillouin zone:

$$[r_n, h(\Pi^{(n)})] = 0. \quad (\text{S13})$$

Thus, there is a common eigenbasis of $h(\Pi^{(n)})$ and r_n :

$$h(\Pi^{(n)}) \left| \epsilon_j(\Pi^{(n)}), p \right\rangle = \epsilon_j(\Pi^{(n)}) \left| \epsilon_j(\Pi^{(n)}), p \right\rangle \quad (\text{S14})$$

$$r_n \left| \epsilon_j(\Pi^{(n)}), p \right\rangle = \Pi_{p,j}^{(n)} \left| \epsilon_j(\Pi^{(n)}), p \right\rangle \quad (\text{S15})$$

where the eigenvalues of r_n at $\Pi^{(n)}$ in energy band band j are

$$\Pi_{p,j}^{(n)} = e^{2\pi i(p-1)/n}, \quad \text{for } p = 1, 2, \dots, n. \quad (\text{S16})$$

The $\Pi_p^{(n)}$ eigenvalues label the C_3 symmetry representations of the eigenstates at the various HSPs. If the eigenvalues within the same band are different for distinct HSPs, that energy band has a nontrivial topology. If they are all the same, the topology is trivial. Therefore, it makes sense to define integer topological invariants as the difference in the number of representations $\Pi_p^{(n)}$ at $\Pi^{(n)}$ and $\Gamma_p^{(n)}$ at the origin $\Gamma = (0, 0)$ of the BZ:

Application to the nonreciprocal Kagome model

The spectrum of the non-Hermitian Hamiltonian

$$q(\mathbf{k}) = \begin{pmatrix} 0 & \kappa_{\text{intra}} & \kappa_{\text{inter}} e^{i\mathbf{k}\cdot\mathbf{a}_1} \\ \kappa_{\text{inter}} e^{i\mathbf{k}\cdot\mathbf{a}_2} & 0 & \kappa_{\text{intra}} \\ \kappa_{\text{intra}} & \kappa_{\text{inter}} e^{i\mathbf{k}\cdot\mathbf{a}_3} & 0 \end{pmatrix}. \quad (\text{S17})$$

under PBC has three bulk bands, which we label as 1, 2, and 3, starting from the positive real axis and going counterclockwise in Figs. 2 (b-d) of the main text. If $|\varepsilon_2(\mathbf{k})\rangle$ is an eigenstate of $q(\mathbf{k})$ belonging to band 2 with energy $\varepsilon_2(\mathbf{k})$, then the time-reversed state $\Theta |\varepsilon_2(\mathbf{k})\rangle = |\varepsilon_3(-\mathbf{k})\rangle$ is an eigenstate in band 3 with energy $\varepsilon_3(-\mathbf{k}) = \varepsilon_2^*(\mathbf{k})$. In other words, time reversal changes the sign of the crystal momentum and maps a given band onto its mirror image relative to the real axis. Since band 1 is its own mirror image, TRS takes $\varepsilon_1(\mathbf{k})$ to $\varepsilon_1(-\mathbf{k}) = \varepsilon_1^*(\mathbf{k})$. Moreover, TRS maps a given eigenstate of the C_3 rotation operator with eigenvalue $e^{2\pi i(p-1)/3}$ onto another eigenstate with the complex-conjugate representation $e^{-2\pi i(p-1)/3}$. One may visually verify all these statements by looking at the location of the HSPs on the spectrum in Figs. 2(b-d) of the main text or checking how TRS and C_3 symmetries constrain the spectrum of $q(\mathbf{k})$.

Table 1: C_3 eigenvalues at HSPs for $\kappa = \kappa_{\text{intra}}/\kappa_{\text{inter}} < 1$ (topological phase).

Point	Band 1	Band 2	Band 3
\mathbf{K}	$K_3 = e^{-2\pi i/3}$	$K_2 = e^{2\pi i/3}$	$K_1 = 1$
\mathbf{K}'	$K'_2 = e^{2\pi i/3}$	$K'_1 = 1$	$K'_3 = e^{-2\pi i/3}$
Γ	$\Gamma_1 = 1$	$\Gamma_3 = e^{-2\pi i/3}$	$\Gamma_2 = e^{2\pi i/3}$

Table 2: C_3 eigenvalues at HSPs for $\kappa = \kappa_{\text{intra}}/\kappa_{\text{inter}} > 1$ (trivial phase).

Point	Band 1	Band 2	Band 3
\mathbf{K}	$K_1 = 1$	$K_2 = e^{2\pi i/3}$	$K_3 = e^{-2\pi i/3}$
\mathbf{K}'	$K'_1 = 1$	$K'_2 = e^{2\pi i/3}$	$K'_3 = e^{-2\pi i/3}$
Γ	$\Gamma_1 = 1$	$\Gamma_2 = e^{2\pi i/3}$	$\Gamma_3 = e^{-2\pi i/3}$

Constraints on the topological invariants:

- There is one HSP Π of each kind for each band i , all having different C_3 representations. The set of bands

Table 3: C_3 topological invariants for $\kappa = \kappa_{\text{intra}}/\kappa_{\text{inter}} < 1$ (nontrivial phase).

Invariant	Band 1	Band 2	Band 3
$[K_1]$	-1	0	1
$[K_2]$	0	1	-1
$[K_3]$	1	-1	0
$[K'_1]$	-1	1	0
$[K'_2]$	1	0	-1
$[K'_3]$	0	-1	1

Table 4: C_3 topological invariants for $\kappa = \kappa_{\text{intra}}/\kappa_{\text{inter}} > 1$ (trivial phase).

Invariant	Band 1	Band 2	Band 3
$[K_1]$	0	0	0
$[K_2]$	0	0	0
$[K_3]$	0	0	0
$[K'_1]$	0	0	0
$[K'_2]$	0	0	0
$[K'_3]$	0	0	0

spans all C_3 eigenvalues. Therefore,

$$\sum_i [\Pi_p]_i = 0 - 1 + 1 = 0 \quad (\text{S18})$$

- Another constraint is

$$\sum_p [\Pi_p]_i = 0, \quad (\text{S19})$$

because $\sum_p \#\Pi_{p,i} = \sum_p \#\Gamma_{p,i}$.

- TRS maps the HSPs as

$$\mathbf{K} \mapsto \mathbf{K}', \quad \mathbf{K}' \mapsto \mathbf{K}, \quad \Gamma \mapsto \Gamma.$$

Moreover, it maps the energy bands as

$$2 \mapsto 3, \quad 3 \mapsto 2, \quad 1 \mapsto 1$$

and the C_3 eigenvalues as

$$\Pi_1 = 1 \mapsto 1 = \Pi_1, \quad \Pi_2 = e^{2\pi i/3} \mapsto e^{-2\pi i/3} = \Pi_3, \quad \Pi_3 \rightarrow \Pi_2.$$

Therefore, we must have

$$\begin{aligned} \#K_{1,1} &= \#K'_{1,1}, & \#K_{2,1} &= \#K'_{3,1}, & \#K_{3,1} &= \#K'_{2,1}, \\ \#K_{1,2} &= \#K'_{1,3}, & \#K_{2,2} &= \#K'_{3,3}, & \#K_{3,2} &= \#K'_{2,3}, \\ \#K_{1,3} &= \#K'_{1,2}, & \#K_{2,3} &= \#K'_{3,2}, & \#K_{3,2} &= \#K'_{2,3}, \\ \#\Gamma_{2,1} &= \#\Gamma_{3,1}, & \#\Gamma_{1,2} &= \#\Gamma_{1,3}, & \#\Gamma_{2,2} &= \#\Gamma_{3,3}, & \#\Gamma_{3,2} &= \#\Gamma_{2,3}. \end{aligned}$$

These relations imply the following constraints on the topological invariants:

$$\begin{aligned}[K_1]_1 &= [K'_1]_1, & [K_1]_2 &= [K'_1]_{2*}, & [K_1]_3 &= [K'_1]_2, \\ [K_2]_1 &= [K'_3]_1, & [K_2]_2 &= [K'_3]_{2*}, & [K_2]_3 &= [K'_3]_2, \\ [K_3]_1 &= [K'_2]_1, & [K_3]_2 &= [K'_2]_{2*}, & [K_3]_3 &= [K'_2]_2,\end{aligned}\quad (\text{S20})$$

The constraint conditions (S18), (S19), and (S20) mean that the independent topological invariants are $\chi^{(3)} = ([K_1]_1, [K_1]_2, [K_2]_1, [K_2]_2) = (-1, 0, 0, 1)$ for the topological phase and $(0, 0, 0, 0)$ for the trivial phase.

After taking into account all the constraints in Eqs. (S18–S20), we obtain an index $\chi^{(3)} = ([K_1]_1, [K_1]_2, [K_2]_1, [K_2]_2)$ consisting of four independent topological invariants that determine the phase of the system. It takes the values $\chi^{(3)} = (-1, 0, 0, 1)$ for the topological phase and $\chi^{(3)} = (0, 0, 0, 0)$ for the trivial phase.

S3 The coupled-model theory for the unidirectional coupling of two coupled acoustic cavities

Suppose two acoustic cavities (resonators) are connected by a unidirectional coupling κ_0 . The tight-binding model Hamiltonian is

$$H_2 = \begin{pmatrix} \omega_0 & 0 \\ \kappa_0 & \omega_0 \end{pmatrix}. \quad (\text{S21})$$

Here, $\text{Re}(\omega_0)$ is the first resonant (angular) frequency of a single cavity, $-\text{Im}(\omega_0) > 0$ is the intrinsic loss, and κ_0 is the unidirectional coupling realized by the active components. In general, $\kappa_0 \in \mathbb{C}$ is a complex number.

Based on the coupled-mode theory, the dynamic equation for this system with a source excitation $|s\rangle$ is

$$i \frac{d|\psi(t)\rangle}{dt} = H |\psi(t)\rangle + |s(t)\rangle, \quad (\text{S22})$$

where $|\psi(t)\rangle = [\psi_1(t) \quad \psi_2(t)]^T$ is the time-dependent sound pressure vector.

For a harmonic excitation at an angular frequency ω , the excitation and sound pressure vectors can be written as $|s(t)\rangle = |s\rangle e^{-i\omega t}$ and $|\psi(t)\rangle = |\psi\rangle e^{-i\omega t}$, respectively. The dynamic equation (S22) is then expressed as

$$(\omega - H) |\psi\rangle = |s\rangle. \quad (\text{S23})$$

When the source is excited at cavity 1, the excitation vector is $|s\rangle = \psi_{\text{in}} [1 \quad 0]^T$, where ψ_{in} is the complex amplitude. Consequently, the sound pressure distribution is obtained by solving Eq. (S23) to give

$$|\psi(t)\rangle = \psi_{\text{in}} e^{-i\omega t} \begin{bmatrix} 1 & \kappa_0 \\ \omega - \omega_0 & (\omega - \omega_0)^2 \end{bmatrix}^T. \quad (\text{S24})$$

To determine the phase of the unidirectional coupling κ_0 , the cross-power spectral density between two measured signals is calculated in experiments

$$G(\omega) \equiv \frac{\psi_2(\omega)}{\psi_1(\omega)} = \frac{\kappa_0}{\omega - \omega_0}. \quad (\text{S25})$$

It is observed that, when $\omega = \text{Re}(\omega_0)$, the phase of G and κ_0 follows the relation

$$\angle G(\text{Re}(\omega_0)) = \angle \kappa_0 - \frac{\pi}{2}. \quad (\text{S26})$$

Supplementary Figures

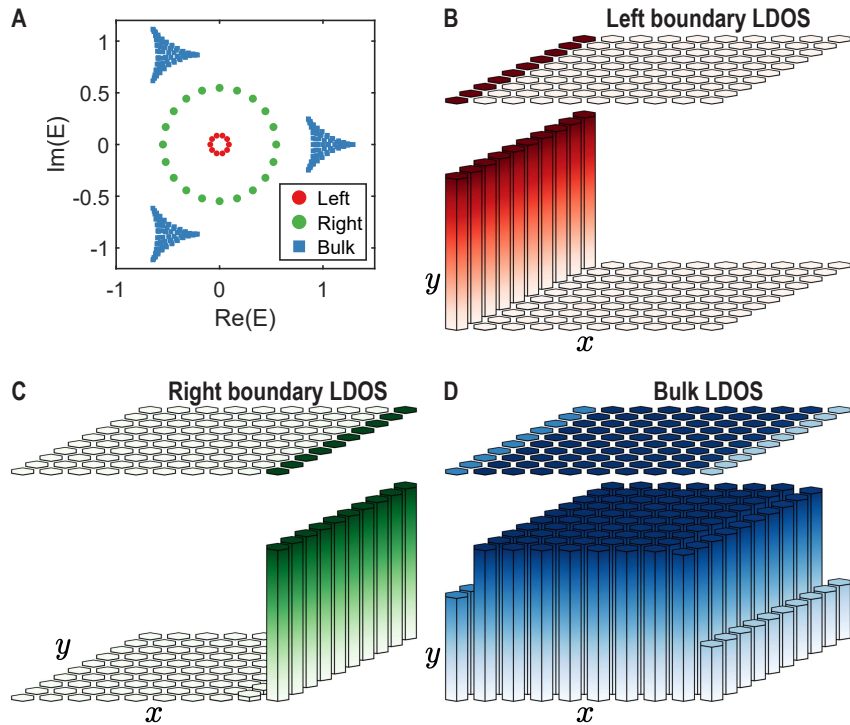


Figure S1: Non-Hermitian Kagome lattice with OBC along the x -direction and PBC along the y -direction, with $\kappa = 0.3$. **(A)** Energy spectrum, with states localized at $x = 1$ and $x = L_x = 10$ shown in red and green, respectively, and bulk states shown in blue. **(B–D)** LDOS for the **(B)** left boundary, **(C)** right boundary, and **(D)** bulk states per unit cell.

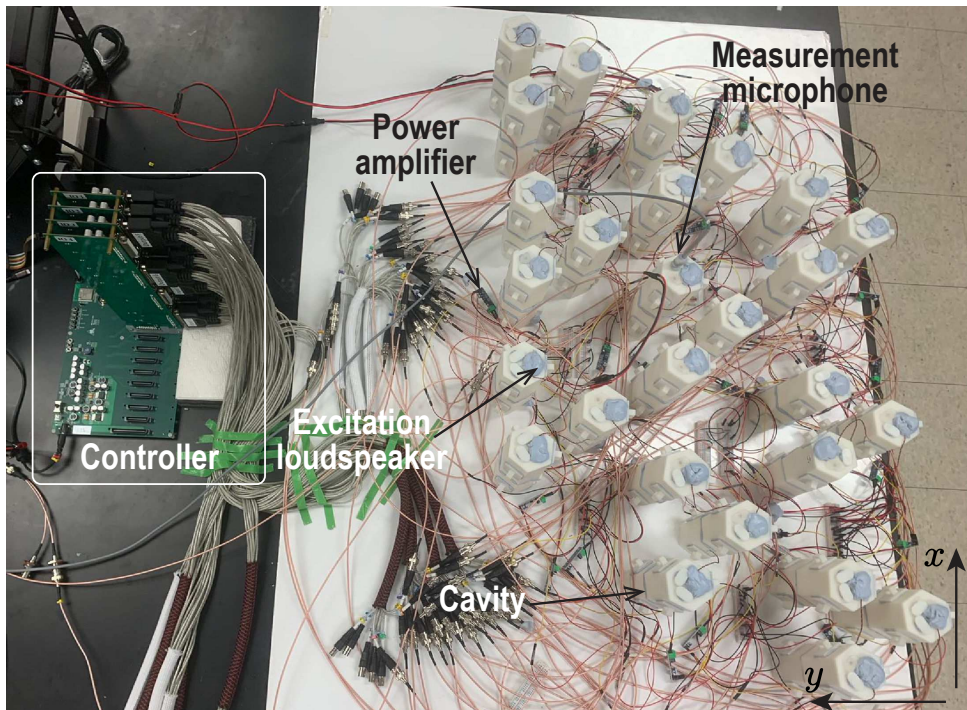


Figure S2: Photo of the experiment setup. We use 27 3D-printed acoustic cavities to represent sites of the non-Hermitian Kagome lattice. The unidirectional hoppings among cavities are realized by source-detector pairs as illustrated in Fig. 5 in the main text. The hopping strength as well as the phase are tuned based on a digital multi-channel controller.

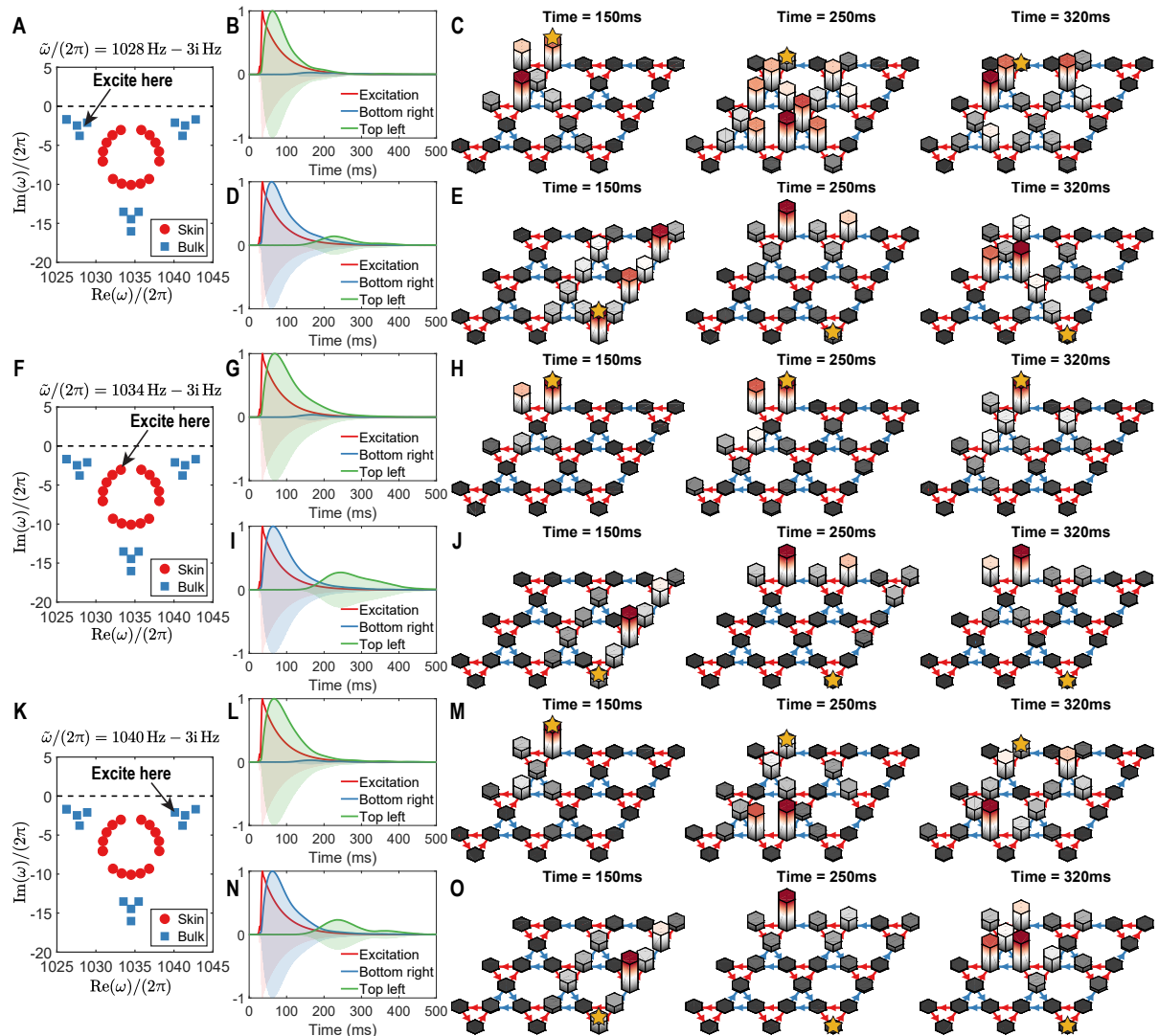


Figure S3: Experimental demonstration in a nontrivial Kagome lattice with dimensions $L_x = L_y = 3$ and hopping parameters $\kappa = 0.5$ and $\kappa_{\text{inter}}/(2\pi) = \kappa_{\text{intra}}/\pi = 7.43e^{-i\pi/2} \text{ Hz}$. (A, F, K) The complex eigenfrequencies showing the CFE at (A) $\tilde{\omega}/(2\pi) = 1028 \text{ Hz} - 3i \text{ Hz}$, (F) $\tilde{\omega}/(2\pi) = 1034 \text{ Hz} - 3i \text{ Hz}$, and (K) $\tilde{\omega}/(2\pi) = 1040 \text{ Hz} - 3i \text{ Hz}$. The lattice is excited by a loudspeaker (denoted by a yellow star \star) at a cavity in the (B, C, G, H, L, M) top left and (D, E, I, J, N, O) bottom right unit cells. (B, D, G, I, L, N) The excitation signal and signals measured at the cavity in the top left and bottom right unit cells as a function of time. (C, E, H, J, M, O) Acoustic energy distributions measured at 150 ms, 250 ms, and 320 ms.

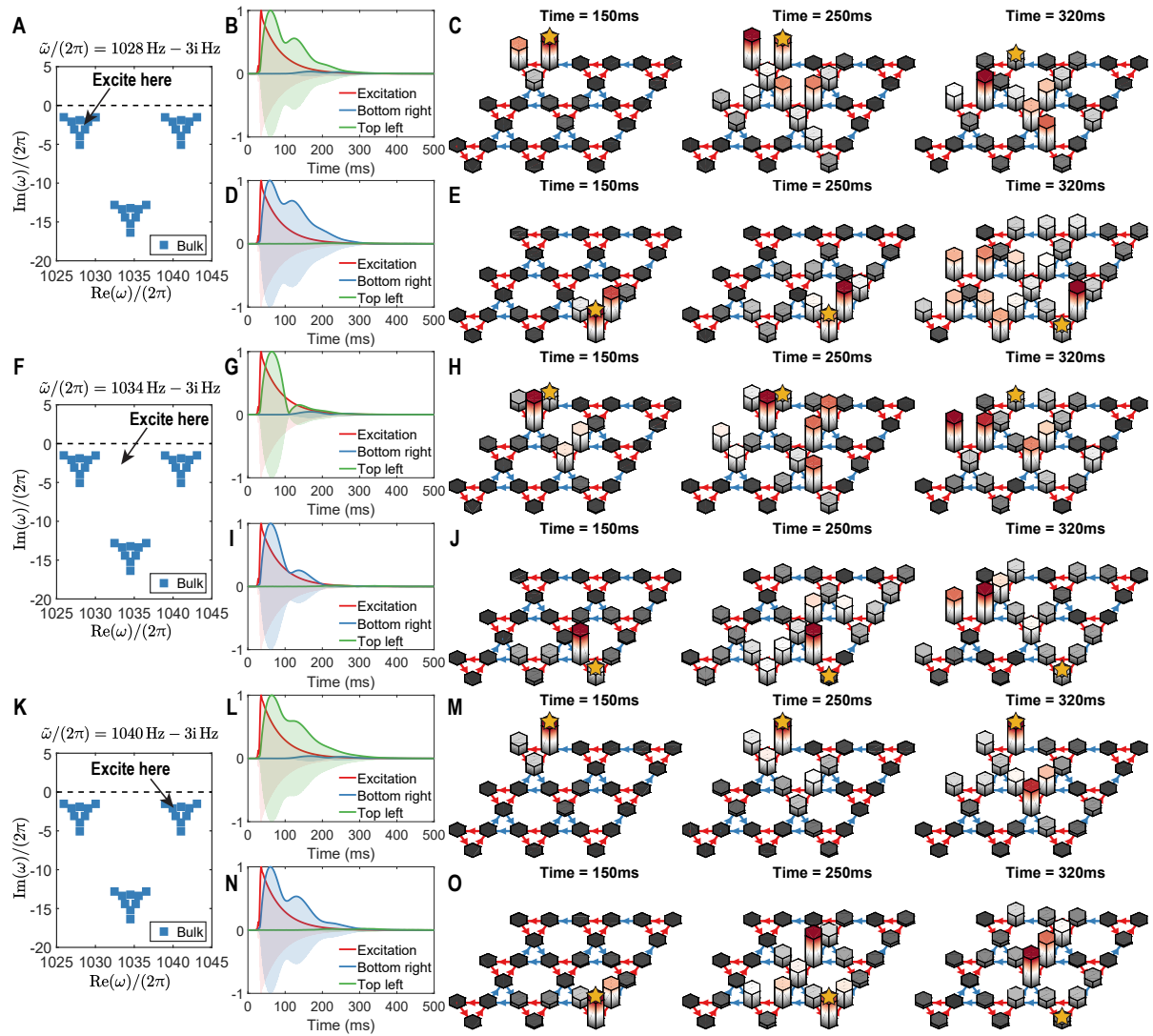


Figure S4: Experimental demonstration in a trivial Kagome lattice with dimensions $L_x = L_y = 3$ and hopping parameters $\kappa = 2$ and $\kappa_{\text{intra}}/(2\pi) = \kappa_{\text{inter}}/\pi = 7.43e^{-i\pi/2} \text{ Hz}$. **(A, F, K)** The complex eigenfrequencies showing the CFE at **(A)** $\tilde{\omega}/(2\pi) = 1028 \text{ Hz} - 3i \text{ Hz}$, **(F)** $\tilde{\omega}/(2\pi) = 1034 \text{ Hz} - 3i \text{ Hz}$, and **(K)** $\tilde{\omega}/(2\pi) = 1040 \text{ Hz} - 3i \text{ Hz}$. The lattice is excited by a loudspeaker (denoted by a yellow star \star) at a cavity in the **(B, C, G, H, L, M)** top left and **(D, E, I, J, N, O)** bottom right unit cells. **(B, D, G, I, L, N)** The excitation signal and signals measured at the cavity in the top left and bottom right unit cells as a function of time. **(C, E, H, J, M, O)** Acoustic energy distributions measured at 150 ms, 250 ms, and 320 ms.

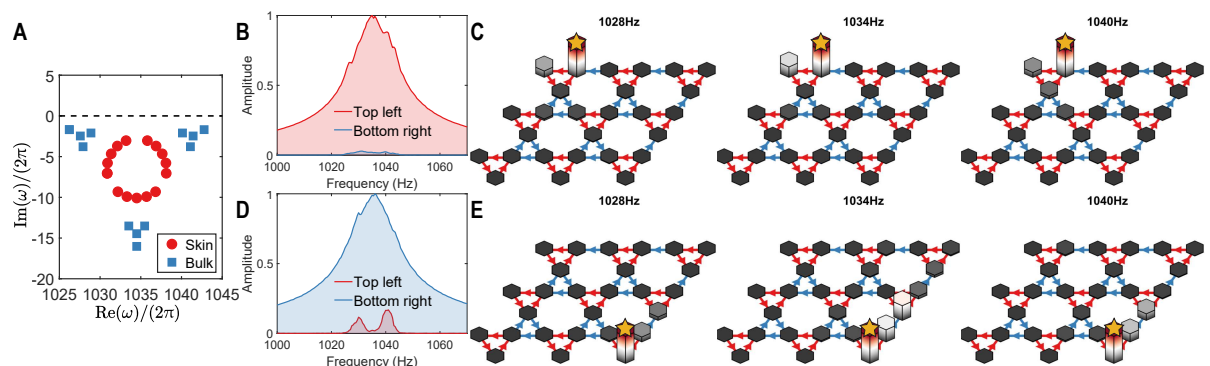


Figure S5: Experimental demonstration with real-frequency excitation in a nontrivial Kagome lattice with dimensions $L_x = L_y = 3$ and hopping parameters $\kappa = 0.5$ and $\kappa_{\text{inter}}/(2\pi) = \kappa_{\text{intra}}/\pi = 7.43e^{-i\pi/2} \text{ Hz}$. **(A)** The complex eigenfrequency of the lattice. The lattice is excited by a loudspeaker (denoted by a yellow star \star) at a cavity in the **(B, C)** top left and **(D, E)** bottom right unit cells. **(B, D)** The excitation signal and signals measured at the cavity in the top left and bottom right unit cells as a function of the excitation frequency. **(C, E)** Acoustic energy distributions measured at 1028 Hz, 1034 Hz, and 1040 Hz.

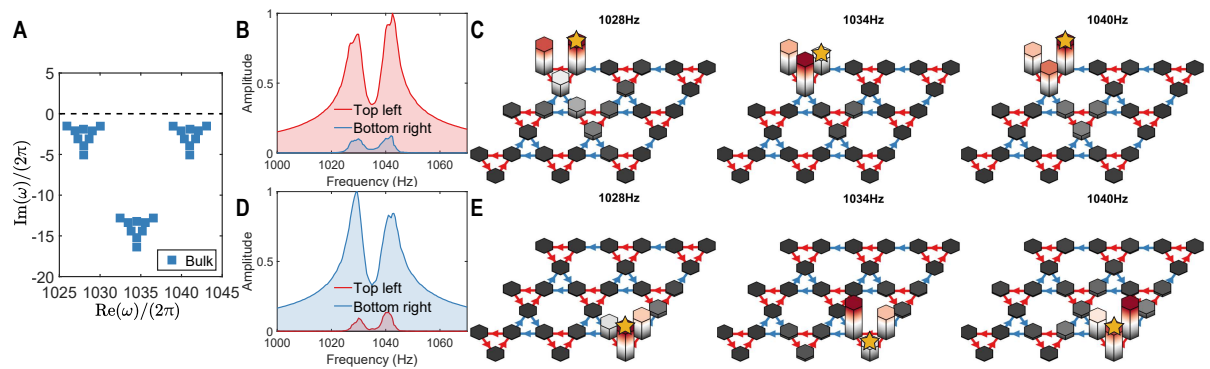


Figure S6: Experimental demonstration with real-frequency excitation in a nontrivial Kagome lattice with dimensions $L_x = L_y = 3$ and hopping parameters $\kappa = 0.5$ and $\kappa_{\text{intra}}/(2\pi) = \kappa_{\text{inter}}/\pi = 7.43e^{-i\pi/2}$ Hz. (A) The complex eigenfrequency of the lattice. The lattice is excited by a loudspeaker (denoted by a yellow star \star) at a cavity in the (B, C) top left and (D, E) bottom right unit cells. (B, D) The excitation signal and signals measured at the cavity in the top left and bottom right unit cells as a function of the excitation frequency. (C, E) Acoustic energy distributions measured at 1028 Hz, 1034 Hz, and 1040 Hz.

Supplementary Movies

Movie S1

Time-evolution of the acoustic field under the CFE at $1034 \text{ Hz} - 3i \text{ Hz}$ when excited at a top-left corner cavity of the nontrivial lattice, with intra-cell hopping $\kappa_{\text{intra}}/(2\pi) = 3.72 e^{-i\pi/2} \text{ Hz}$ and inter-cell hopping $\kappa_{\text{inter}}/(2\pi) = 7.43 e^{-i\pi/2} \text{ Hz}$.

Movie S2

Time-evolution of the acoustic field under the CFE at $1034 \text{ Hz} - 3i \text{ Hz}$ when excited at a bottom-right corner cavity of the nontrivial lattice, with intra-cell hopping $\kappa_{\text{intra}}/(2\pi) = 3.72 e^{-i\pi/2} \text{ Hz}$ and inter-cell hopping $\kappa_{\text{inter}}/(2\pi) = 7.43 e^{-i\pi/2} \text{ Hz}$.

Movie S3

Time-evolution of the acoustic field under the CFE at $1028 \text{ Hz} - 3i \text{ Hz}$ when excited at a top-left corner cavity of the nontrivial lattice, with intra-cell hopping $\kappa_{\text{intra}}/(2\pi) = 3.72 e^{-i\pi/2} \text{ Hz}$ and inter-cell hopping $\kappa_{\text{inter}}/(2\pi) = 7.43 e^{-i\pi/2} \text{ Hz}$.

Movie S4

Time-evolution of the acoustic field under the CFE at $1028 \text{ Hz} - 3i \text{ Hz}$ when excited at a bottom-right corner cavity of the nontrivial lattice, with intra-cell hopping $\kappa_{\text{intra}}/(2\pi) = 3.72 e^{-i\pi/2} \text{ Hz}$ and inter-cell hopping $\kappa_{\text{inter}}/(2\pi) = 7.43 e^{-i\pi/2} \text{ Hz}$.

Movie S5

Time-evolution of the acoustic field under the CFE at $1040 \text{ Hz} - 3i \text{ Hz}$ when excited at a top-left corner cavity of the nontrivial lattice, with intra-cell hopping $\kappa_{\text{intra}}/(2\pi) = 3.72 e^{-i\pi/2} \text{ Hz}$ and inter-cell hopping $\kappa_{\text{inter}}/(2\pi) = 7.43 e^{-i\pi/2} \text{ Hz}$.

Movie S6

Time-evolution of the acoustic field under the CFE at $1040 \text{ Hz} - 3i \text{ Hz}$ when excited at a bottom-right corner cavity of the nontrivial lattice, with intra-cell hopping $\kappa_{\text{intra}}/(2\pi) = 3.72 e^{-i\pi/2} \text{ Hz}$ and inter-cell hopping $\kappa_{\text{inter}}/(2\pi) = 7.43 e^{-i\pi/2} \text{ Hz}$.

Movie S7

Time-evolution of the acoustic field under the CFE at $1028 \text{ Hz} - 3i \text{ Hz}$ when excited at a top-left corner cavity of the trivial lattice, with intra-cell hopping $\kappa_{\text{intra}}/(2\pi) = 7.43 e^{-i\pi/2} \text{ Hz}$ and inter-cell hopping $\kappa_{\text{inter}}/(2\pi) = 3.72 e^{-i\pi/2} \text{ Hz}$.

Movie S8

Time-evolution of the acoustic field under the CFE at $1028 \text{ Hz} - 3i \text{ Hz}$ when excited at a bottom-right corner cavity of the trivial lattice, with intra-cell hopping $\kappa_{\text{intra}}/(2\pi) = 7.43 e^{-i\pi/2} \text{ Hz}$ and inter-cell hopping $\kappa_{\text{inter}}/(2\pi) = 3.72 e^{-i\pi/2} \text{ Hz}$.

Movie S9

Time-evolution of the acoustic field under the CFE at $1034 \text{ Hz} - 3i \text{ Hz}$ when excited at a top-left corner cavity of the trivial lattice, with intra-cell hopping $\kappa_{\text{intra}}/(2\pi) = 7.43 e^{-i\pi/2} \text{ Hz}$ and inter-cell hopping $\kappa_{\text{inter}}/(2\pi) = 3.72 e^{-i\pi/2} \text{ Hz}$.

Movie S10

Time-evolution of the acoustic field under the CFE at $1034 \text{ Hz} - 3i \text{ Hz}$ when excited at a bottom-right corner cavity of the trivial lattice, with intra-cell hopping $\kappa_{\text{intra}}/(2\pi) = 7.43 e^{-i\pi/2} \text{ Hz}$ and inter-cell hopping $\kappa_{\text{inter}}/(2\pi) = 3.72 e^{-i\pi/2} \text{ Hz}$.

Movie S11

Time-evolution of the acoustic field under the CFE at $1040 \text{ Hz} - 3i \text{ Hz}$ when excited at a top-left corner cavity of the trivial lattice, with intra-cell hopping $\kappa_{\text{intra}}/(2\pi) = 7.43 e^{-i\pi/2} \text{ Hz}$ and inter-cell hopping $\kappa_{\text{inter}}/(2\pi) = 3.72 e^{-i\pi/2} \text{ Hz}$.

Movie S12

Time-evolution of the acoustic field under the CFE at $1040 \text{ Hz} - 3i \text{ Hz}$ when excited at a bottom-right corner cavity of the trivial lattice, with intra-cell hopping $\kappa_{\text{intra}}/(2\pi) = 7.43 e^{-i\pi/2} \text{ Hz}$ and inter-cell hopping $\kappa_{\text{inter}}/(2\pi) = 3.72 e^{-i\pi/2} \text{ Hz}$.

References

- [1] N. Hatano and D. R. Nelson, “Localization Transitions in Non-Hermitian Quantum Mechanics,” *Phys. Rev. Lett.*, vol. 77, no. 3, pp. 570–573, Jul. 15, 1996.
- [2] N. Hatano and D. R. Nelson, “Vortex pinning and non-Hermitian quantum mechanics,” *Phys. Rev. B*, vol. 56, no. 14, pp. 8651–8673, Oct. 1, 1997.
- [3] K. Kawabata, M. Sato, and K. Shiozaki, “Higher-order non-Hermitian skin effect,” *Phys. Rev. B*, vol. 102, no. 20, p. 205118, Nov. 17, 2020.